Supplementary Data for

Effect of off-stoichiometric composition on half-metallic character of $Co_2Fe(Ga,Ge)$ investigated using saturation magnetization and giant magnetoresistance effect

§1. Optimization of layer structures and annealing condition for CFGG-based GMR devices

Before investigating the Ge-composition dependence of MR ratios, we optimized layer structures and annealing condition for CFGG-based GMR devices. Figure S1 shows MR ratios as functions of (a) the thickness of upper CFGG layer (t_{CFGG}), (b) the thickness of NiAl insertion layer (t_{NiAl}), and (c) annealing temperature (T_a). From these figures, we determined t_{CFGG} = 8 nm, t_{NiAl} = 0.21 nm, and T_a = 550˚C.

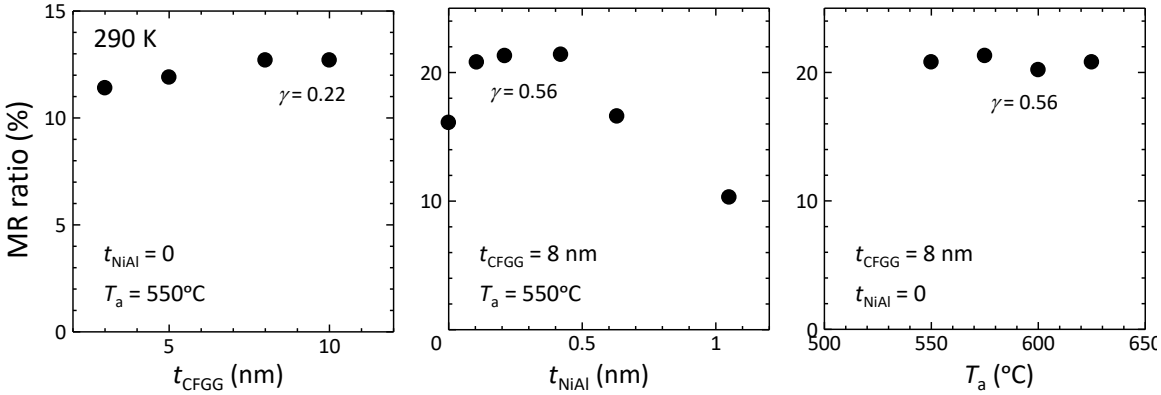

Fig. S1. MR ratios as functions of (a) t_{CFGG}, (b) t_{NiAl}, and (c) T_a. The Ge composition γ in $Co_2Fe_{1.03}Ga_{0.41}Ge_\gamma$ is 0.22 or 0.56.

§2. Site-specific formula unit (SSFU) composition model for CFGG

The SSFU model describes how many atoms occupy at each atomic site under thermodynamically stable conditions. In case for CFGG, we assumed that ordinary atomic arrangement (Co_{Co}, Fe_{Fe}, $(Ga,Ge)_{(Ga,\ Ge)}$) and some antisites (Co_{Fe}, Fe_{Co}, $Fe_{(Ga,Ge)}$, $(Ga,Ge)_{Fe}$) were assumed in determining the atomic arrangement, where X_Y indicates X atom occupies Y site, because these formation energies are lower than those of other atomic arrangements or vacancies. We now derive the type-I SSFU composition for off-stoichiometric composition of $Co_2Fe_\alpha Ga_\beta Ge_\gamma$. In the type I, Co_{Fe} and $(Ga,Ge)_{Fe}$ antisites are formed, resulting in the SSFU composition of $[Co_2][Co_xFe_{1-x-y}(Ga_{1-\xi}Ge_\xi)_y][Ga_{1-\xi}Ge_\xi]$, where the Co site is occupied by Co only, the Fe site is occupied by Co, Fe, and (Ga,Ge), and the (Ga,Ge) site is occupied by (Ga,Ge). Note that total number of occupied atom at each site is always 2, 1, and 1, because no vacancies are assumed. Since each atomic ratio should be kept between $Co_2Fe_\alpha Ga_\beta Ge_\gamma$ and $[Co_2][Co_xFe_{1-x-y}(Ga_{1-\xi}Ge_\xi)_y][Ga_{1-\xi}Ge_\xi]$, the following relation is satisfied:

$$\text{Co : Fe : Ga : Ge} = 2 : \alpha : \beta : \gamma = (2+x) : (1-x-y) : (1-\xi)(y+1) : \xi(y+1) \quad \text{(S1)}$$

From eq.(S1), we get

$$x = 2\{2-(\alpha+\beta+\gamma)\}/(2+\alpha+\beta+\gamma),$$

$$y = \{3(\beta + \gamma) - (2 + \alpha)\}/(2 + \alpha + \beta + \gamma) \quad \text{(S2)}$$

$$\xi = \gamma/(\beta + \gamma).$$

Depending on the sign of x and y in eq.(S1), different kinds of antisites are formed. If $x > 0$ and $y < 0$ are satisfied, then antisites of Co_{Fe} and $Fe_{(Ga,Ge)}$ are formed, resulting in the type-II SSFU composition of $[Co_2][Co_xFe_{1-x}][Fe_{|y|}(Ga_{1-\xi}Ge_{\xi})_{1-|y|}]$. Similarly, the case for $x < 0$ and $y > 0$ results in the type-III SSFU composition of $[Co_{2-|x|}Fe_{|x|}][Fe][Fe_y(Ga_{1-\xi}Ge_{\xi})_{1-y}]$, where antisites of Fe_{Co} and $Fe_{(Ga,Ge)}$ are formed. The case for $x < 0$ and $y < 0$ results in the type-IV SSFU composition of $[Co_{2-|x|}Fe_{|x|}][Fe_{1-|y|}(Ga_{1-\xi}Ge_{\xi})_{|y|}][Ga_{1-\xi}Ge_{\xi}]$, where antisites of Fe_{Co} and $(Ga,Ge)_{Fe}$ are formed.

§3. Structural analysis of CFGG thin films by X-ray diffraction

Figure S3 shows XRD θ-2θ scan for $Co_2Fe_{1.03}Ga_{0.45}Ge_\gamma$ (γ = 0.24, 0.56, 0.96, 1.25, and 1.54) thin films. Clear 004 and 002 diffraction peaks of CFGG were observed in all the samples, indicating that the CFGG films are $L2_1$-ordered or B2-ordered. Moreover, no other peaks arising from segregation was observed.

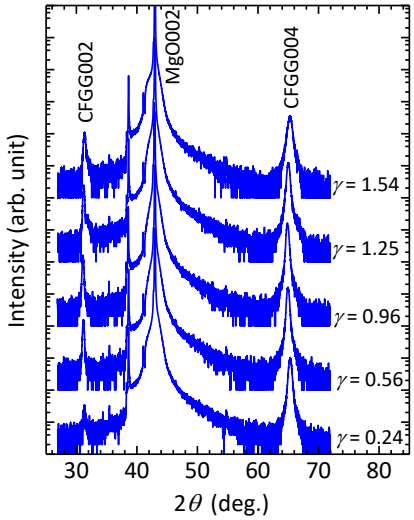

Fig. S2. XRD θ-2θ scan for $Co_2Fe_{1.03}Ga_{0.45}Ge_\gamma$ (γ = 0.24, 0.56, 0.96, 1.25, and 1.54) thin films.

§4. Structure factor of electron or X-ray diffractions

Table S1 summarizes structure factor for 111, 200, and 400 diffractions, where f_{Co}, f_{Fe}, and $f_{(Ga,Ge)}$ are the atomic form factors of Co, Fe, and (Ga,Ge), respectively. 400 diffraction is allowed for all structures of $L2_1$, B2, and A2. 200 diffraction is allowed for $L2_1$ and B2, and 111 diffraction is allowed only for $L2_1$ structure.

Table S1. Structure factor for 111, 200, and 400 diffractions

	$L2_1$	B2	A2
111	$f_{Fe} - f_{(Ga,Ge)}$	0	0
200	$2f_{Co} - (f_{Fe} + f_{(Ga,Ge)})$	$2f_{Co} - (f_{Fe} + f_{(Ga,Ge)})$	0
400	$2f_{Co} + (f_{Fe} + f_{(Ga,Ge)})$	$2f_{Co} + (f_{Fe} + f_{(Ga,Ge)})$	$2f_{Co} + (f_{Fe} + f_{(Ga,Ge)})$

§5. Typical MR curves of CFGG-based GMR devices with various Ge composition

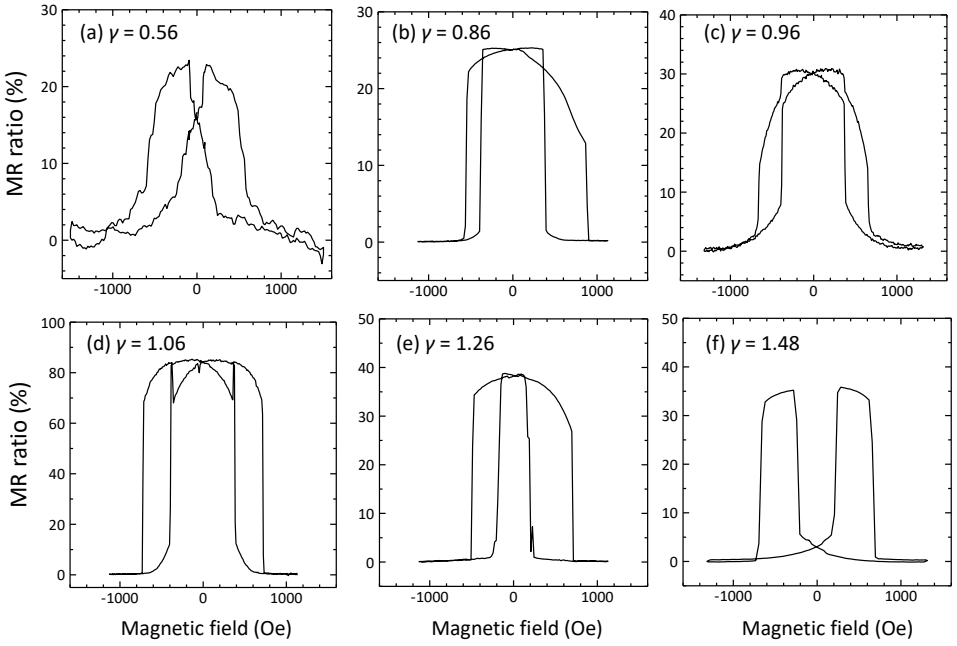

Fig. S3. Typical MR curves of series-B and series-C GMR devices.

§6. Bias-current dependence of MR ratio

Figure S5 shows (a) current (I) - voltage (V) characteristics for parallel (P) and anti-parallel (AP) configuration between upper and lower CFGG electrodes, (b) typical MR curves at $I = -0.2$ mA, -2 mA and +2 mA, and (c) bias-current dependences of R_P, R_{AP}, and MR ratio, measured at 290 K for a series-B GMR device with $\gamma = 1.06$. The bias voltage is defined with respect to the lower CFGG electrode, and electrons

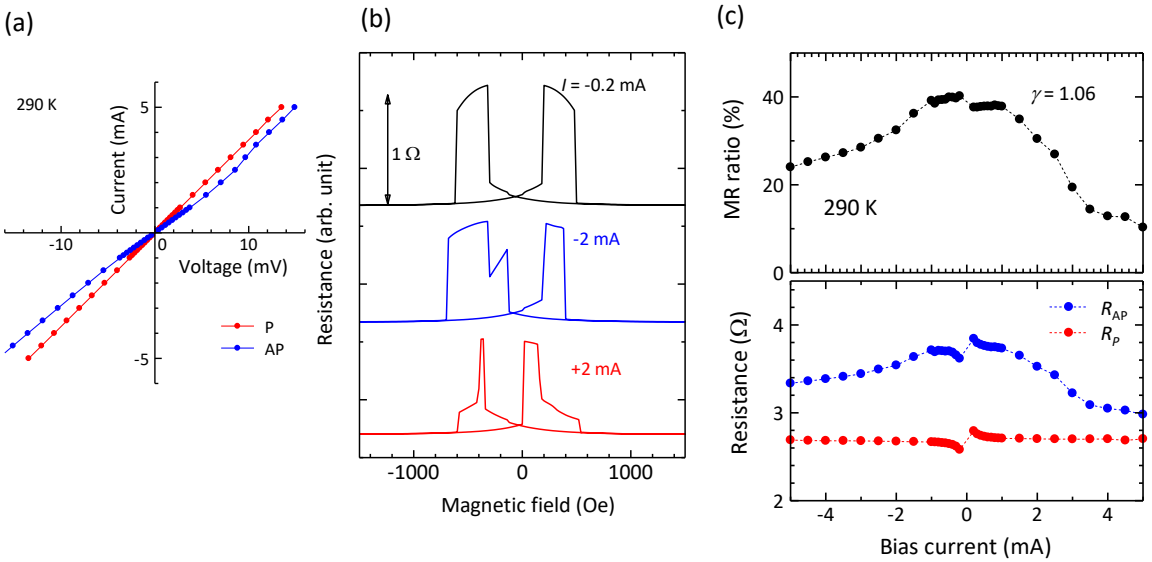

Fig. S4. (a) I-V characteristics, (b) typical MR curves at $I = -0.2$ mA, -2 mA and +2 mA, and (c) bias-current dependences of R_P, R_{AP}, and MR ratio, for a series-B GMR device with $\gamma = 1.06$. The MR curves are offset for clarity.

flow from lower CFGG into upper CFGG under positive bias. Almost linear *I-V* curves were obtained for both P and AP configurations. As increasing $|I|$, the R_{AP} decreased monotonically, while R_P was almost constant, resulting in that the MR ratio decreased monotonically. The R_{AP} and MR ratio decreased faster with positive *I* than with negative *I*. This is because the spin transfer torque exerts the magnetization of upper CFGG under positive bias, resulting in favoring the P configuration.

§7. Temperature dependence of MR ratio

Figure S6 shows (a) typical MR curves at temperature (T) = 10 K, 150 K, and 290 K, and (b) temperature dependence of R_P, R_{AP}, and MR ratio, for a series-B GMR devices with γ = 1.06. The MR ratio increased with decreasing T from 290 K to 10 K as would be expected from spin-dependent transport in GMR devices. In more detail, an increase in the spin polarization of the CFGG electrodes and suppression of spin-flip transport via thermally exited magnons in GMR stacks with decreasing T lead to a decrease in R_P and an increase in R_{AP}.

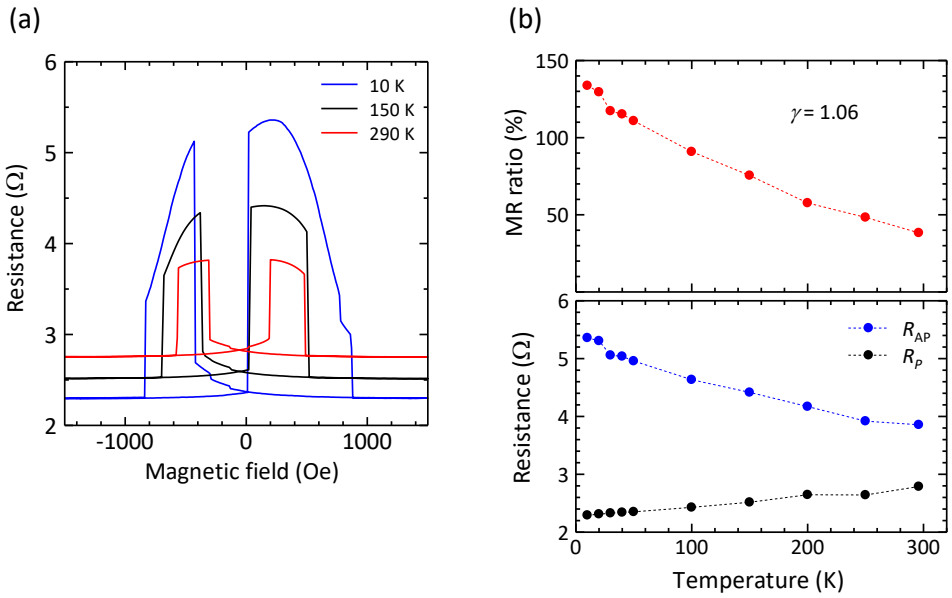

Fig. S5. (a) typical MR curves at T = 10 K, 150 K, and 290 K, (b) temperature dependence of R_P, R_{AP}, and MR ratio, for a series-B GMR device with γ = 1.06.

§8. SSFU model with B2-type disorder

Theoretical calculations were performed for atomic arrangements determined by SSFU compositions with B2-type disorder, in which the atomic arrangement for the Fe site and (Ga,Ge) site is randomized. Table S2 summarizes the comparison of original SSFU compositions described in section S2 and those with B2-type disorder for $Co_2Fe_{1.03}Ga_{0.41}Ge_\gamma$. The first, second and third bracket in the original SSFU composition indicate the original Co site, Fe site, and (Ga,Ge) site in the $L2_1$ structure, respectively, whereas the first and second bracket in the SSFU compositions with B2-type disorder indicate the original Co site and (Fe, Ga, Ge) site, respectively. Note that Fe site and (Ga,Ge) site cannot be distinguished in the SSFU with B2-type disorder.

Table S2. Comparison of original SSFU compositions and those with B2-type disorder for $Co_2Fe_{1.03}Ga_{0.41}Ge_\gamma$.

γ	Original SSFU	SSFU with B2-type disorder
0.24	$[Co_2][Fe_{0.826}Co_{0.174}][Ga_{0.446}Ge_{0.261}Fe_{0.293}]$	$[Co_2][Fe_{1.119}Co_{0.174}Ga_{0.446}Ge_{0.261}]$
0.56	$[Co_2][Fe][Ga_{0.410}Ge_{0.560}Fe_{0.03}]$	$[Co_2][Fe_{1.03}Ga_{0.446}Ge_{0.261}]$
0.96	$[Co_{1.818}Fe_{0.182}][Fe_{0.755}Ga_{0.073}Ge_{0.172}][Ga_{0.299}Ge_{0.701}]$	$[Co_{1.818}Fe_{0.182}][Fe_{0.755}Ga_{0.372}Ge_{0.873}]$
1.25	$[Co_{1.706}Fe_{0.294}][Fe_{0.584}Ga_{0.103}Ge_{0.313}][Ga_{0.247}Ge_{0.753}]$	$[Co_{1.706}Fe_{0.294}]$ $[Fe_{0.584}Ga_{0.343}Ge_{1.066}]$
1.54	$[Co_{1.606}Fe_{0.394}][Fe_{0.434}Ga_{0.119}Ge_{0.447}][Ga_{0.210}Ge_{0.790}]$	$[Co_{1.606}Fe_{0.394}]$ $[Fe_{0.434}Ga_{0.329}Ge_{1.237}]$

§9. Depth profiles of constituent atoms investigated through energy dispersive x-ray spectroscopy

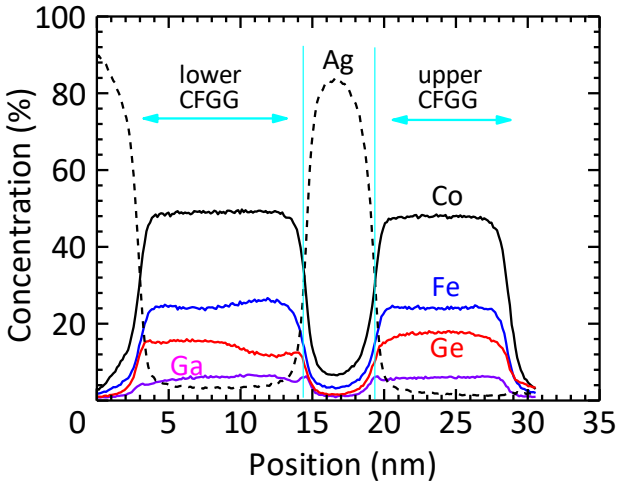

Fig. S6. Depth profiles of Co, Fe, Ga, Ge, and Ag for a series-B GMR device with $\gamma = 1.06$.